Available online at www.sciencedirect.com
ScienceDirect
International Journal of Heat and Mass Transfer 50 (2007) 3877–3889
International Journal of HEAT and MASS TRANSFER
www.elsevier.com/locate/ijhmt

Spectral Monte Carlo models for nongray radiation analyses in inhomogeneous participating media

Anquan Wang, Michael F. Modest *

Department of Mechanical and Nuclear Engineering, Pennsylvania State University, University Park, PA 16802, USA

Received 22 October 2006; received in revised form 3 February 2007
Available online 16 April 2007

Abstract

A spectral line-by-line (LBL) method is developed for photon Monte Carlo simulations of radiation in participating media. The performance of the proposed method is compared with that of the stochastic full-spectrum k-distribution (FSK) method in both homogeneous and inhomogeneous media, and in both traditional continuum media and media represented by stochastic particle fields, which are frequently encountered in combustion simulations. By using random-number relations, the LBL method does its own spectral reordering, in effect similar to the FSK reordering. Both LBL and FSK methods result in the same level of statistical errors for similar numbers of photon bundles. It is shown that the FSK approach is superior to the LBL approach in both memory and CPU efficiency in all test cases. However, the CPU efficiency is not prominent when spectral calculations are not the dominant source of overall CPU-time cost. Due to a lack of correlation of absorption coefficients in inhomogeneous media, the FSK approach may produce substantial errors, which are avoided by the LBL method. The LBL database can be constructed once and for all, while the FSK database has to be reconstructed every time the reference state changes. Thus, the LBL method is more suitable for quickly-evolving media.

Keywords: Monte Carlo; Nongray; Participating media; Thermal radiation

1. Introduction

Radiation of participating media has great influence on heat transfer in many high-temperature applications, such as combustion problems. A variety of radiative transfer models has been developed to deal with radiation in participating media. Among them the photon Monte Carlo (PMC) method can handle problems of high complexity with relative ease. Based on random-number relations, histories of energy bundles are traced to simulate the physical processes, such as emission, scattering, absorption, etc., and the result approaches the exact solution with diminishing statistical error with increasing numbers of energy bundles. Well-known disadvantages of this method are its high computational costs and statistical scatter. However, these become less important with the rapid increase of computational capacity of computers.

Early PMC studies often assumed gases to be gray, such as Howell and Perlmutter's work [1], which appears to be the first application of PMC methods in radiative heat transfer. However, the gray-gas assumption may yield unacceptable errors in many engineering applications, since for most gases the spectral variation of radiative properties is very strong. The first modern study on nongray gases using the PMC method was made by Modest [2] in 1992, who developed random-number relations based on a statistical narrow-band model to take spectral line structure into account. Similar methods were employed in several other PMC studies since then. Liu and Tiwari [3] used a statistical narrow-band model with an exponential-tailed-inverse intensity distribution in the investigation of radiative dissipation inside the medium and net radiative wall heat flux for different temperature and concentration profiles in a 1D problem. Cherkaoui et al. [4] used the statistical

* Corresponding author. Fax: +1 814 863 4848.
E-mail address: mfm6@psu.edu (M.F. Modest).

0017-9310/$ - see front matter © 2007 Elsevier Ltd. All rights reserved.
doi:10.1016/j.ijheatmasstransfer.2007.02.018

Nomenclature

A	boundary (wall) area
a	nongray stretching factor in FSK method
g	cumulative k-distribution
I	number of species; radiative intensity
I_b	blackbody radiative intensity
k	absorption coefficient variable
L	cylinder length
N_{ray}	number of rays per run
N_{wv}	number of wavenumbers (or g's) per ray
$\hat{\mathbf{n}}$	local boundary surface normal
p	pressure
$\mathbf{q}$	local radiative heat flux vector
$\bar{q}$	averaged boundary flux
R	random number; cylinder radius
s	position variable along ray path
T	temperature
t_{cpu}	average CPU time per run
x	mole fraction
x, y, z, r	coordinates

Greek symbols

η	wavenumber
Φ	scattering phase function
$\underline{\phi}$	gas state variable
κ	absorption coefficient
κ_p	pressure-based Planck-mean absorption coefficient
Ω'	solid angle
σ	Stefan–Boltzmann constant; standard deviation
σ_s	scattering coefficient
τ	optical thickness

Subscripts

0	reference state
η	spectral
i	species index

narrow-band model in a 1D slab problem with prescribed temperature fields and the reciprocity principle was employed to reduce the statistical error. Farmer and Howell [5,6] developed random-number relations based on an exponential wide band absorption profile to treat nongray emission and absorption of carbon dioxide. Most recently, Wang et al. [7] incorporated the full-spectrum k-distribution (FSK) method, the most promising nongray model for deterministic solvers, into the PMC method in an artificial 1D problem. Tang and Brewster [8] used the line-by-line (LBL) method, the most accurate spectral model, combined with PMC to serve as benchmark for other wideband and narrow-band models in a 1D homogeneous medium. In their work, rather than developing random-number relations to determine wavenumbers, spectral integrations are used to give total radiative quantities. Nevertheless, to our knowledge, it is the only work combining the LBL and PMC methods.

Recently, the PMC method has been implemented in several CFD simulations of combustion, due to the continuous improvements in numerical methods and computer capabilities. Snegirev [9] incorporated a PMC method into a CFD code with the weighted-sum-of-gray-gases (WSGG) model in his study of buoyant turbulent nonpremixed flames. Tessé et al. [10,11] developed their PMC methods to model the radiative transfer in a turbulent sooty flame, in which a narrow-band correlated-k model was used for spectral integration. For a variety of combustion applications, in which joint probability-density-function (PDF) methods [12,13] are used, the medium is represented by statistical particles evolving with time, and traditional Monte Carlo ray-tracing methods developed for continuous media are no longer useful. Most recently, Wang and Modest [14,15] developed several emission and absorption schemes for discrete particle fields, which can be utilized to perform PMC simulations in such media. The PMC method has also been applied in a variety of other participating media. For example, Xia et al. [16] developed a curved Monte Carlo method for radiative heat transfer in media with variable index of refraction. Ruan et al. [17] applied the Monte Carlo method in media with nongray absorbing–emitting-anisotropic scattering particles, and Mazumder and Kersch [18] employed a Monte Carlo scheme for thermal radiation in semiconductor processing applications.

The present paper proposes a spectral LBL approach, based on random-number relations, to be incorporated into PMC models for nongray radiation analyses in combustion gases. By using random-number relations, the wavenumbers with substantial emission are more likely to be chosen. Therefore, it is expected that fewer wavenumbers are required to yield accuracy comparable to the one obtained from standard spectral integration. The LBL method is compared with the PMC/FSK approach in terms of CPU efficiency, memory requirements, accuracy, statistical errors, etc., using several sample calculations.

2. Theoretical development

2.1. Photon Monte Carlo method

Gas molecules in a combustion medium continuously emit energy in the form of photons into random directions at distinct wavenumbers, which are determined by the energy difference between the two quantized energy levels of an emitting molecule before and after emission. Photons may be absorbed or scattered by other molecules during

transmission. Photon Monte Carlo (PMC) methods directly simulate such processes by releasing representative photons bundles (rays) into random directions, which are traced until they are absorbed at certain points in the medium or escape from the domain. In traditional continuous media photon rays carry a fixed amount of energy and the optical thickness they can travel through is determined randomly as

$$\tau_o = \ln(1/R_\tau), \quad \tau_o = \int_0^{s^*} \kappa \, ds, \tag{1}$$

where τ_o is the predetermined optical thickness for a specific ray, R_τ is the random number uniformly distributed in $[0,1)$, s is the position variable along the path and s^* is the location at which the ray is absorbed. Starting from the emission location, the optical thickness passed through by a ray is accumulated during tracing until its corresponding τ_o value is reached, then all the energy carried by the ray is absorbed by the subvolume at the absorbing location. This method is called the *standard* Monte Carlo method. If the medium is optically thin, most of the rays may exit open boundaries without contributing to the statistics in the medium. Similarly, if the medium is optically very thick, rays travel only very short distances without contributing to statistics of elements far away. In both cases the standard method becomes very inefficient. An alternative, the *energy partitioning* method, was proposed to alleviate such problem [19,20], in which the ray energy is absorbed gradually and partitioned to all the subvolumes it traverses until depletion or exiting. Both standard and energy partitioning methods can also be implemented in media represented by statistical particles, in which the ray energy is absorbed by a single particle when the optical thickness reaches its predetermined value in the standard method, or the energy is distributed over all particles that the ray interacts with in the energy partitioning method [14].

In continuous media emission points of rays are determined randomly according to the emissive energy distribution in the domain. In hot zones of combustion gases the concentrations of carbon dioxide and water vapor tend to be high and strong emission is observed. Thus, hot zones must be represented by more rays than cold zones with weak emission, and the ray number density reflects the emissive energy distribution, which is achieved by constructing random-number relations for emission locations [21]. By inverting such random-number relations, the emission location can be determined as

$$x = x(R_x), \quad y = y(R_y, x), \quad z = z(R_z, x, y), \tag{2}$$

where R_x, R_y and R_z are independent random numbers. In media represented by particle fields rays are emitted from the inside of particles and particle centers can be chosen as emission points if particles are small [14]. Since particles may emit different amounts of energy, the particle energy may be split into several rays in hot zones and several particle energies may be combined together to emit a single ray in cold zones, to constrain ray energy to a small range and minimize statistical error [15].

The determination of isotropic emission directions is identical for both continuous media and media represented by particle fields, using random-number relations that emit rays into all directions with equal probability. For gray analyses the Planck-mean absorption coefficient is used in calculations and no spectral modeling is required. For non-gray analyses wavenumbers carried by photon bundles must be randomly determined according to a certain random-number relation, which is the focus of the present paper. In standard simulations each photon bundle is assigned a single but different wavenumber. If the number of rays required to resolve spectral variations is much larger than the number of rays required to resolve spacial variations in the problem, it may be advantageous to assign multiple wavenumbers to each ray and thus trace fewer rays to reduce computational time. While equal energies are initially given to each wavenumber, the required path-length in ray-tracing is different for different wavenumbers due to the spectral variation of absorption coefficients and/or the different predetermined optical thickness for each wavenumber. Therefore, the tracing of a photon bundle carrying multiple wavenumbers is not completed until its energies associated with all wavenumbers are absorbed or it exits the domain.

For either continuous media or media represented by particle fields, random-number relations can also be constructed for scattering in conventional ways, if required [21].

2.2. Spectral random-number relations

The probability of the number of photons emitted in a differential wavenumber interval $d\eta$ is proportional to the Planck function weighted by the spectral absorption coefficient, i.e.,

$$\text{Probability}\{\eta \text{ in } d\eta\} \propto \kappa_\eta I_{b\eta} \, d\eta, \tag{3}$$

where η denotes the wavenumber, κ_η is the corresponding local spectral absorption coefficient and $I_{b\eta}$ is the spectral blackbody intensity. Therefore, to simulate this emission process of photons statistically for a given gas species i, the random-number relation for the emission wavenumber is derived as

$$R_{\eta,i} = \frac{\int_0^\eta \kappa_{\eta,i} I_{b\eta} \, d\eta}{\int_0^\infty \kappa_{\eta,i} I_{b\eta} \, d\eta} = \frac{\int_0^\eta \kappa_{p\eta,i} I_{b\eta} \, d\eta}{\int_0^\infty \kappa_{p\eta,i} I_{b\eta} \, d\eta} = \frac{\pi}{\kappa_{p,i} \sigma T^4} \int_0^\eta \kappa_{p\eta,i} I_{b\eta} \, d\eta, \tag{4}$$

where $R_{\eta,i}$ is a random number uniformly distributed in $[0,1)$, $\kappa_{p\eta,i} = \kappa_{\eta,i}/p_i$ is the pressure-based spectral absorption coefficient and p_i is the partial pressure of species i; $\kappa_{p,i}$ is the pressure-based Planck-mean absorption coefficient, σ is the Stefan–Boltzmann constant and T is the gas temperature. Since Eq. (4) is an implicit relation

between the random number and the wavenumber, it is more convenient to tabulate this relation in a database to invert random numbers into emission wavenumbers.

In practice one deals with gas mixtures. Considering that the absorption coefficient is additive,

$$\kappa_\eta = \sum_i \kappa_{\eta,i} = \sum_i \kappa_{\mathrm{p}\eta,i} p_i \quad \text{and}$$
$$\kappa_{\mathrm{p}\eta} = \kappa_\eta / p = \sum_i x_i \kappa_{\mathrm{p}\eta,i}, \tag{5}$$

where $x_i = p_i/p$ is the mole fraction of species i and p is the total pressure of the mixture, one can obtain the random-number relation for the gas mixture from Eq. (4) as

$$\begin{aligned} R_\eta &= \frac{\pi}{\kappa_{\mathrm{p}} \sigma T^4} \int_0^\eta \kappa_{\mathrm{p}\eta} I_{\mathrm{b}\eta}\, \mathrm{d}\eta \\ &= \frac{\pi}{\sigma T^4 \sum_i x_i \kappa_{\mathrm{p},i}} \int_0^\eta \sum_i x_i \kappa_{\mathrm{p}\eta,i} I_{\mathrm{b}\eta}\, \mathrm{d}\eta \\ &= \frac{\pi}{\sigma T^4 \sum_i x_i \kappa_{\mathrm{p},i}} \sum_i x_i \int_0^\eta \kappa_{\mathrm{p}\eta,i} I_{\mathrm{b}\eta}\, \mathrm{d}\eta \\ &= \sum_i x_i \kappa_{\mathrm{p},i} R_{\eta,i} \Big/ \sum_i x_i \kappa_{\mathrm{p},i}. \end{aligned} \tag{6}$$

Eq. (6) establishes a direct relation between the mixture random number R_η and species random numbers $\{R_{\eta,i}\}$. Since the relation between the mixture random number R_η and the corresponding wavenumber η is implicit, direct inversion from R_η to η through Eq. (6) is impossible and must be done by trial-and-error. For a given wavenumber η, the species random numbers $\{R_{\eta,i}\}$ are first determined, followed by the calculation of R_η through Eq. (6). For absorption calculations, the desired mixture absorption coefficient κ_η at a given wavenumber can be directly calculated from species pressure-based absorption coefficients $\{\kappa_{\mathrm{p}\eta,i}\}$ through Eq. (5). Therefore, a database tabulating both $R_{\eta,i}$–η and $\kappa_{p\eta,i}$–η relations of each species can be utilized to determine emission wavenumbers and absorption coefficients for the mixture, and such a database can be constructed once and for all. If the total pressure is fixed, both the species random number, as in Eq. (4), and the pressure-based absorption coefficient are functions of wavenumber, temperature and species concentration only, i.e.,

$$R_{\eta,i} = f_{R,i}(\eta, T, x_i), \quad \kappa_{\mathrm{p}\eta,i} = f_{\kappa,i}(\eta, T, x_i), \quad i = 1, 2, \ldots, I, \tag{7}$$

where I is the number of species. If self-broadening effects of absorption coefficients are negligible, $R_{\eta,i}$ and $\kappa_{\mathrm{p}\eta,i}$ are functions of temperature and wavenumber only. Thus, a 3D interpolation scheme (2D if self-broadening is neglected) is sufficient for the database and the computational effort increases only linearly with increasing number of species. Fig. 1 shows the random number and corresponding absorption coefficient distributions of a gas mixture in a small spectral interval. Although the random number is a

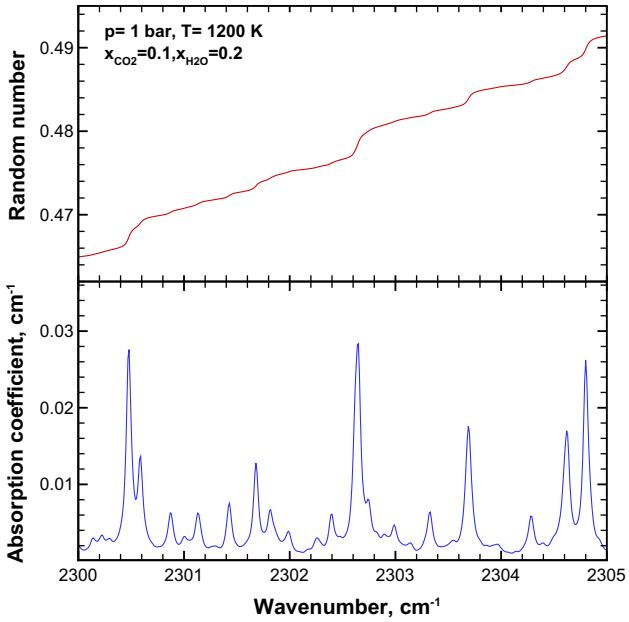

Fig. 1. Random number and absorption coefficient distributions in a small spectral interval (absorption coefficient data obtained from Wang and Modest [27]).

monotonically increasing function, it has strongly varying gradients even in such a small interval. A small error in random number may result in a significant deviation in absorption coefficient. Therefore, common root-finding techniques relying on smooth gradients, such as the Newton–Raphson method, cannot be used here to invert random numbers. Instead, a bisectional search algorithm may be employed in such a process since the R_η–η relation is monotonic, if the resolution of the random number database is sufficient to resolve those steps. Spectral scattering coefficients may also be added into the database if scattering is considered.

In the FSK approach the oscillating absorption coefficient spectrum, κ_η–η, is reordered into a well-behaved monotonic k–g distribution, in which k is the absorption coefficient variable and g is the Planck-function-weighted cumulative density function of k. Correspondingly, by employing the correlated-k assumption, the original radiative transfer equation (RTE) [21]

$$\frac{\mathrm{d}I_\eta}{\mathrm{d}s} = \kappa_\eta (I_{\mathrm{b}\eta} - I_\eta) - \sigma_{\mathrm{s}\eta} \left[I_\eta - \frac{1}{4\pi} \int_{4\pi} I_\eta(\hat{s}') \Phi(\hat{s}, \hat{s}')\, \mathrm{d}\Omega' \right] \tag{8}$$

is mapped into g-space as [22]

$$\begin{aligned} \frac{\mathrm{d}I_g}{\mathrm{d}s} &= k(T_0, \underline{\phi}, g)[a(T, T_0, g) I_{\mathrm{b}} - I_g] \\ &\quad - \sigma_{\mathrm{s}} \left[I_g - \frac{1}{4\pi} \int_{4\pi} I_g(\hat{s}') \Phi(\hat{s}, \hat{s}')\, \mathrm{d}\Omega' \right], \end{aligned} \tag{9}$$

where I_g is the radiative intensity to be solved in g-space, $k(T_0, \underline{\phi}, g)$ is the full-spectrum k-distribution evaluated by reordering absorption coefficients at the local state $\underline{\phi}$ (including temperature, pressure and concentrations) weighted by the Planck function calculated at the reference

temperature T_0, and $a(T,T_0,g)$ is a nongray stretching function reflecting the ratio of two FSK's evaluated at the same state $\underline{\phi}_0$ but using two different Planck-function temperatures, viz., local temperature T and reference temperature T_0,

$$a(T,T_0,g)=\frac{\mathrm{d}g(T,\underline{\phi}_0,k^*)/\mathrm{d}k^*}{\mathrm{d}g(T_0,\underline{\phi}_0,k^*)/\mathrm{d}k^*},\quad k^*=k(T_0,\underline{\phi}_0,g), \tag{10}$$

where k^* corresponds to the given g in the k–g distribution evaluated at the reference state $\underline{\phi}_0$ and Planck-function temperature T_0.

The first term in brackets on the right-hand side of Eq. (9) represents augmentation of I_g due to local emission and the second term in brackets is the attenuation due to local absorption. For the simulation of emission using Monte Carlo methods, the random-number relation for the determination of a cumulative k-distribution value g, acting like an artificial wavenumber, is then derived as [7]

$$\begin{aligned}R_g&=\frac{\int_0^g k(T_0,\underline{\phi},g)a(T,T_0,g)I_\mathrm{b}\,\mathrm{d}g}{\int_0^1 k(T_0,\underline{\phi},g)a(T,T_0,g)I_\mathrm{b}\,\mathrm{d}g}\\&=\frac{\int_0^g k(T_0,\underline{\phi},g)a(T,T_0,g)\,\mathrm{d}g}{\int_0^1 k(T_0,\underline{\phi},g)a(T,T_0,g)\,\mathrm{d}g},\end{aligned} \tag{11}$$

where R_g is the random number and the upper limit g in the numerator is the desired artificial wavenumber of emission. The denominator is the local Planck-mean absorption coefficient evaluated using the correlated-k assumption.

As shown in Eq. (10), the stretching function $a(T,T_0,g)$ does not depend on the k–g distribution at the local gas state $\underline{\phi}$. For truly correlated absorption coefficients, the local emission at state $\underline{\phi}=(p,T,\underline{x})$ can be evaluated exactly using the FSK method, i.e.,

$$\begin{aligned}\int_0^\infty \kappa_\eta(\underline{\phi})I_{\mathrm{b}\eta}(T)\,\mathrm{d}\eta&=\int_0^1 k(T,\underline{\phi},g^*)I_\mathrm{b}(T)\,\mathrm{d}g^*\\&=\int_0^1 k(T_0,\underline{\phi},g)a(T,T_0,g)I_\mathrm{b}(T)\,\mathrm{d}g,\end{aligned} \tag{12}$$

where $g^*(k)$ is the cumulative k-distribution for the local state. However, in reality, absorption coefficients at different gas states are never truly correlated, i.e., the last part of Eq. (12) becomes an approximation. Modest and Zhang [23] observed a maximum error of 4% when they evaluated radiative sources in combustion products. When including radiation from CH_4, the error was less than 5% everywhere except for the inlet region where large amounts of fuel exist. In this region the error was below 10% except for few small spots with large errors [23]. They also observed that the error of the FSK method can be as large as 26% for wall fluxes in a two-layer CO_2–H_2O–N_2 mixture slab bounded by cold black walls, in which both temperature and mole fractions have step changes in the slab [24].

Eq. (11) is an implicit relation and the random-number inversion is conducted by a table-search method as well. Since the process of assembling of FSK's from absorption coefficients is fairly tedious, it is impractical to assemble FSK's during ray-tracing. Instead, R_g, k and a should be tabulated in a database at a given reference state for a set of temperatures and mole fractions before ray-tracing commences. For a given reference state $\underline{\phi}_0$, while the a-function is a function of temperature and g only, both the random number R_g and k are functions of temperature, g and species concentrations,

$$\begin{aligned}R_g&=f_{R_g}(g,T,x_1,x_2,\ldots,x_I),\\k&=f_k(g,T,x_1,x_2,\ldots,x_I).\end{aligned} \tag{13}$$

As a result, the interpolation scheme required by the FSK database is $(I+2)$-dimensional. As the number of species, I, increases, the interpolation algorithm becomes more and more complicated and CPU cost increases exponentially. In addition, as pointed out by Modest and Zhang [23], for poorly correlated gases the reference state can have a strong effect on the accuracy of the FSK approach. Thus, the FSK database must be reconstructed from time to time, if the overall temperature and concentration fields undergo substantial changes with time, which greatly affect the reference state.

3. Construction of random-number databases

A line-by-line random-number database has been constructed for water vapor and carbon dioxide, the two most important combustion gases. The spectroscopic database HITEMP-2000 was used to calculate absorption coefficients of water vapor, while CDSD-1000 was employed for carbon dioxide, since it is considered to be more accurate than HITEMP [25,26]. To resolve the irregularity of the absorption coefficient across the spectrum, the absorption coefficient must be evaluated at close enough spectral locations. In the present work constant spectral spacing is used across the entire spectrum; the resolution is considered fine enough if, when doubling the resolution, the error of the narrow-band-mean absorption coefficient stays below 0.5% in major absorption bands across the entire spectrum [27]. For a given total pressure, the resolution required depends on temperature and mole fraction. At a total pressure of 1 bar, the finest resolution in the present work, 0.004 cm^{-1}, is used for temperatures over 2000 K at mole fractions less than 0.25, while the crudest, 0.01 cm^{-1}, is used for many other temperatures and mole fractions. The absorption coefficient at a specific spectral location is the result of the overlap of nearby broadened spectral lines. At the most frequently encountered pressure in practice (1 bar) Lorentz broadening is the dominant line-broadening mechanism. Since the extent of Lorentz broadening is inversely proportional to the square-root of temperature and additional spectral lines appear at higher temperature levels ("hot lines"), temperature has great influence on the spectral shapes of the absorption coefficient. Thus, 23 temperatures equally-spaced between

300 K and 2500 K are included in the database. In contrast, mole fractions affect line shapes of pressure-based absorption coefficient only through self-broadening, and this effect is fairly small for CO_2, as shown in Fig. 2a, which shows pressure-based absorption coefficients across a small spectral interval at different mole fractions and a temperature of 1200 K for CO_2. However, the self-broadening effect is considerably larger for H_2O, as shown in Fig. 2b, which implies that more mole fractions need to be included in the database for H_2O.

A homogeneous 1D gas slab problem, in which a mixture of nitrogen and CO_2 or H_2O is contained between two parallel cold black walls, was investigated to evaluate self-broadening effects on radiation calculations. It was seen that, for CO_2, neglecting self-broadening resulted in an error of around 0.2% in terms of radiative fluxes for various slab thicknesses. Therefore, a single mole fraction, say 0.0, is sufficient for the database of CO_2. However, the self-broadening effect is much stronger for H_2O, which in the above problem may yield errors as large as several percent. Careful investigation revealed that linear interpolation between mole fractions of 0.0 and 0.5 can bring errors down to below 0.5% for mole fractions in that range, while parabolic interpolation using mole fractions of 0.0, 0.5 and 1.0 results in errors below 0.1% for the entire mole fraction range. Since mole fractions of water vapor above 0.5 are unlikely in combustion problems, two mole fractions, 0.0 and 0.5, are sufficient for the database.

Since at least 1.5 million wavenumbers are required to describe the oscillating absorption coefficient for the whole spectrum, and since both the random number and the absorption coefficient at each wavenumber must be stored in the database, the LBL approach requires a substantial amount of memory. For two species (CO_2 and H_2O) and 23 temperatures, it takes roughly 1.2 GB of memory to store the whole database in single precision. Keeping in mind that each gas has spectral windows across which the absorption coefficient is negligible, the database can be compressed considerably by storing absorbing bands only. While the absorption coefficient of H_2O is non-negligible across most parts of the spectrum, the absorption bands of CO_2 occupy only a small portion of the spectrum. By adopting this method, the size of the H_2O database was reduced from 768 MB to 657 MB and for CO_2 reduced from 384 MB to 160 MB. More work can be done to improve the memory efficiency of the LBL approach, if desired. It is also worth noting that, since a constant spectral resolution is used for the entire spectrum, fetching data for a given wavenumber becomes quite efficient since its index can be simply calculated.

A gas mixture of 10% CO_2 and 20% H_2O was employed to validate the constructed species random number and absorption coefficient database. Emission wavenumbers determined from the database using random numbers must represent the distribution of spectral emissive energy of the mixture. In Fig. 3a the solid curve is the exact distribution of the normalized spectral emissive energy in spectral intervals ($\delta\eta = 0.01\ \mathrm{cm}^{-1}$), the integrant in Eq. (6), over a small wavenumber range, while the dashed curve is the corresponding Monte Carlo result using 10 million random numbers for the entire spectrum. The Monte Carlo result follows the exact curve with small statistical errors, which will further diminish if the number of random numbers is increased. In Fig. 3b the mixture absorption coefficient as interpolated from the proposed database lies on top of the curve calculated directly from HITEMP and CDSD.

In contrast, the FSK approach is much more efficient in terms of memory. Since change of concentrations may greatly affect the accuracy of a k-distribution, not less than 10 mole fractions for each species are required in building

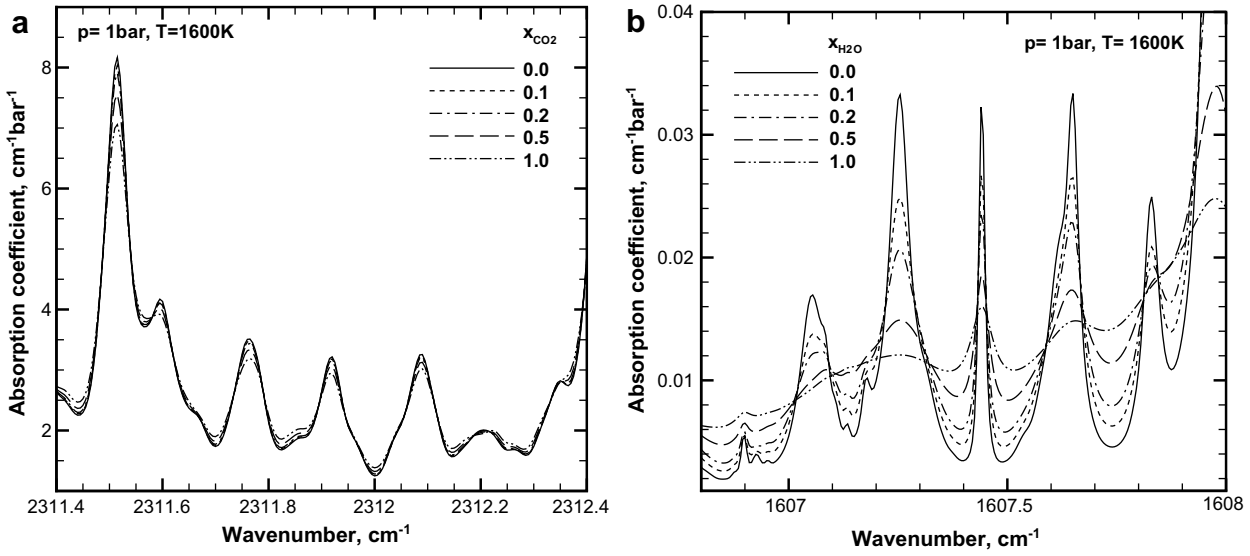

Fig. 2. Pressure-based absorption coefficient in a small spectral interval (obtained from Wang and Modest [27]): (a) CO_2 and (b) H_2O.

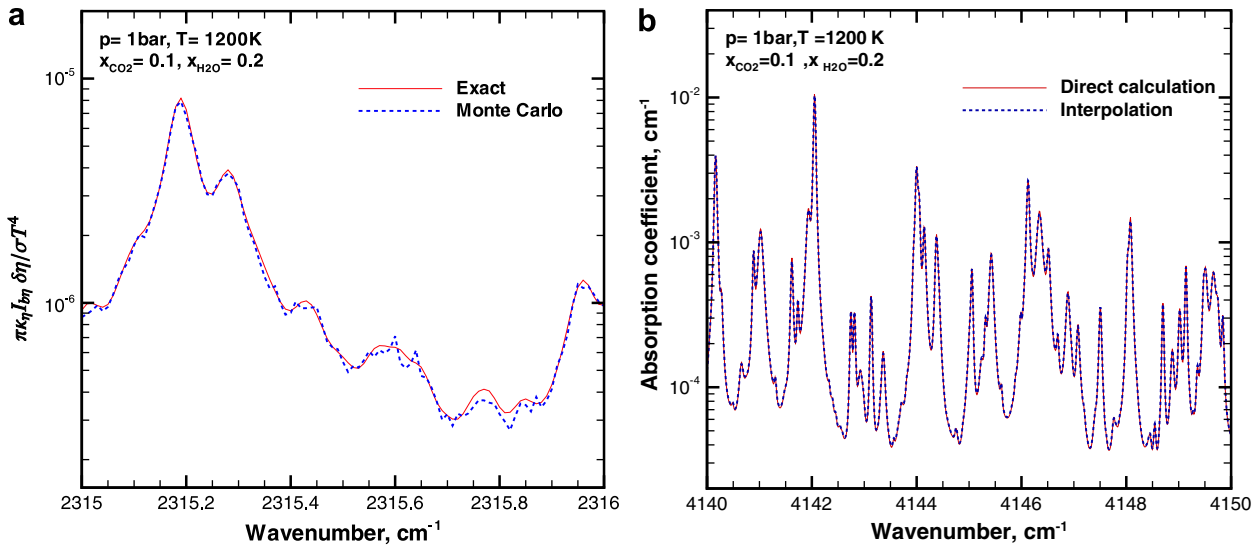

Fig. 3. Normalized spectral emissive energy and pressure-based absorption coefficient in small spectral intervals at different mole fractions.

the FSK random-number database. For 2 species, 23 temperatures and 11 mole fractions, the total arrays of random numbers, k-values and stretching factors require only about 4 MB, if as many as 64 points are stored for each distribution. In the present work FSK's are assembled from a high-accuracy compact narrow-band k-distribution database developed by Wang and Modest [28], to avoid the inefficient direct assembly from absorption coefficients. Unlike the LBL database, which can be constructed once and for all, the FSK database depends on the reference state of the gas mixture and must be constructed for the problem at hand, and must be reconstructed whenever the reference state is changed appreciably.

4. Sample calculations

The PMC/LBL and PMC/FSK implementations are compared in several sample calculations. First, a problem involving a 2D axisymmetric homogeneous CO_2–H_2O–N_2 mixture, surrounded by cold black walls, is considered. The gas temperature is set to a uniform 1620 K and mole fractions of CO_2 and H_2O of 1.4% and 2.8%, respectively, are considered (i.e., the reference state of a methane/air flame discussed later in this section). The radius and length are set to $R = 25$ cm and $L = 100$ cm. Both the PMC/LBL and PMC/FSK methods are implemented in an energy-partitioning Monte Carlo solver designed for 2D axisymmetric continuum media as posted on the website of Modest's text [29]. The side wall is divided into four equal-sized rings, which are numbered together with the two end surfaces as shown in Fig. 4, and radiative fluxes are investigated using both PMC/LBL and PMC/FSK methods. For each run, a certain total number (N_{ray}) of photon rays is traced and each ray carries a number (N_{wv}) of wavenumbers (or g's) randomly determined using the discussed random-number databases. A 64-bit 2.4 GHz AMD Opteron

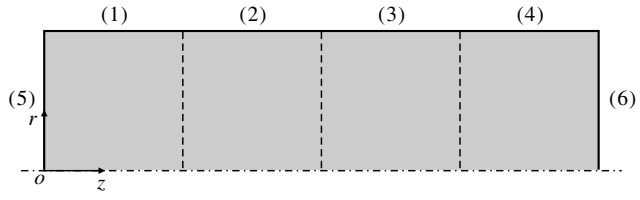

Fig. 4. Wall numbering.

880 CPU was used for all the simulations in the present paper.

For given numbers of rays and wavenumbers (or g's) per ray, the standard deviations of averaged wall fluxes are evaluated from 50 runs using different random-number sequences. The purpose of using such a large number of runs is to accurately evaluate standard deviations and the averaged CPU time per run. The averaged wall flux used here is defined as

$$\bar{q} = \frac{1}{A}\int_A \mathbf{q}\cdot\hat{\mathbf{n}}\,\mathrm{d}A, \tag{14}$$

where $\mathbf{q}$ is the local heat flux vector at the wall, A is the wall area and $\hat{\mathbf{n}}$ is its surface normal. Table 1 lists the standard deviations σ (relative to the mean value $\langle\bar{q}\rangle$) corresponding to each wall flux as well as the averaged simulation time for a single run, using either the LBL or the FSK approach. For each averaged wall flux $\bar{q}$, the relative standard deviation is defined as

$$\sigma = \frac{1}{\langle\bar{q}\rangle}\left[\frac{1}{N-1}\sum_{n=1}^{N}\left(\bar{q}^{(n)} - \langle\bar{q}\rangle\right)^2\right]^{1/2} \quad \text{and}$$

$$\langle\bar{q}\rangle = \frac{1}{N}\sum_{n=1}^{N}\bar{q}^{(n)}, \tag{15}$$

where $N = 50$ is the total number of runs and $\bar{q}^{(n)}$ is the averaged wall flux in the nth run. The mean values of aver-

Table 1
Relative standard deviations of wall fluxes and averaged CPU time per simulation; 50 runs; homogeneous medium problem

N_{ray}	N_{wv}	Relative standard deviations (%)						t_{cpu} (s)
		σ_1	σ_2	σ_3	σ_4	σ_5	σ_6	
(a) LBL approach								
30,000	1	1.47	1.54	1.39	1.42	1.96	2.15	0.337
	4	1.51	1.29	1.38	1.32	2.02	1.87	1.325
60,000	1	0.898	0.948	0.852	0.915	1.40	1.46	0.697
	4	0.954	0.831	0.981	0.957	1.50	1.35	2.577
120,000	1	0.710	0.700	0.589	0.716	0.954	1.13	1.358
(b) FSK approach								
30,000	1	1.33	1.25	1.28	1.36	1.69	2.21	0.093
	4	1.05	1.15	1.29	1.07	1.95	2.36	0.258
60,000	1	1.04	0.915	0.832	1.075	1.31	1.51	0.188
	4	0.831	0.752	0.897	0.882	1.32	1.39	0.517
120,000	1	0.764	0.642	0.600	0.778	1.07	1.21	0.377

N_{ray}, number of rays per run; N_{wv}, number of wavenumbers per ray; t_{cpu}, average CPU time per run.

aged wall fluxes are $\langle \bar{q}_1 \rangle = \langle \bar{q}_4 \rangle = 1.41\ \mathrm{W/cm^2}$, $\langle \bar{q}_2 \rangle = \langle \bar{q}_3 \rangle = 1.65\ \mathrm{W/cm^2}$ and $\langle \bar{q}_5 \rangle = \langle \bar{q}_6 \rangle = 1.33\ \mathrm{W/cm^2}$, using 200,000 rays for both LBL and FSK approaches, since the FSK approach is exact for homogeneous media. Different values of N_{ray} are used in simulations to investigate the effects of number of rays per run, and different values of N_{wv} are tried with the expectation that more wavenumbers per ray might yield smaller statistical errors without significant increase in CPU time. In nongray analyses the statistical error results from spatial uncertainty, due to random emission locations and directions, and from spectral uncertainty due to random wavenumbers (or g's) approximating the spectrum. It is observed that, while standard deviations are inversely proportional to the square-root of the number of rays N_{ray} as expected, effects of the number of wavenumbers N_{wv} on standard deviations are minor, which implies that spatial uncertainty is the major cause for the statistical error, and that the spectral variation of radiative intensities can be well resolved even with as few as 30,000 photon bundles per run in this problem. As a result, the combination of 120,000 rays per run with 1 wavenumber per ray has only one half the standard deviation as compared to the combination of 30,000 rays per run with 4 wavenumbers per ray, with a similar cost of CPU time. Table 1 shows that both LBL and FSK approaches achieve the same level of statistical error. It appears that the PMC/LBL approach does its own spectral reordering, given by Eq. (6), in effect similar to the FSK reordering. The FSK approach is much more efficient in terms of CPU time as expected, since spatial calculations are fairly simple and spectral calculations dominate the cost of CPU time in this homogeneous problem. Even though the LBL spectrum contains 100,000 times as many data points as a full-spectrum k-distribution, the LBL approach is only 3–4 times slower than the FSK approach for given values of N_{ray} and N_{wv} as shown in Table 1. This is expected, since a bisectional search algorithm is used in database queries. For an ordered table containing n entries, the average number of comparisons using a bisectional search algorithm is $\log_2 n$. Therefore, for a LBL spectrum containing 1.5–3 million wavenumbers, the average number of data comparisons per query is around 21, while, for a 64-point k-distribution, the average number of comparisons is 6 per query.

To test the PMC/LBL and PMC/FSK methods in inhomogeneous media, the medium in the previous problem is replaced by a two-layer medium with step changes of temperature and concentrations in the radial direction. A hot core ($r \leqslant R/2$) at 1600 K contains 10% of CO_2 and 5% of H_2O, surrounded by a cold layer ($R/2 < r \leqslant R$) at 500 K containing 5% of CO_2 and 10% of H_2O, respectively. The correlation of absorption coefficient is expected to break down in such problems with substantial gradients in temperature and/or concentrations. The uncorrelatedness of emission and absorption states results in a larger number of spectral random numbers required to resolve both emission and absorption, as shown in Table 2. For a given combination of N_{ray} and N_{wv}, standard deviations in the inhomogeneous problem are noticeably greater than those in the homogeneous problem. As a result, unlike in the homogeneous problem, increasing N_{wv} also decreases the

Table 2
Relative standard deviations of wall fluxes in the inhomogeneous medium problem (50 runs)

N_{ray}	N_{wv}	Relative standard deviations (%)					
		σ_1	σ_2	σ_3	σ_4	σ_5	σ_6
(a) LBL approach							
30,000	1	2.35	2.05	2.14	2.28	2.22	2.46
	4	1.21	1.58	1.43	1.36	2.03	2.04
60,000	1	1.77	1.55	1.29	1.78	1.68	1.91
	4	0.900	1.13	1.08	1.17	1.53	1.47
120,000	1	1.31	1.09	0.922	1.04	1.22	1.26
(b) FSK approach							
30,000	1	1.98	1.67	1.77	2.12	2.33	2.93
	4	1.46	1.39	1.42	1.57	2.12	2.52
60,000	1	1.54	1.24	1.25	1.41	1.72	1.94
	4	1.01	0.866	0.877	1.19	1.50	1.45
120,000	1	1.12	0.932	1.02	1.08	1.26	1.47

standard deviation. However, the increase of N_{wv} is still not as effective as increasing N_{ray}, since the latter reduces both spatial and spectral uncertainties at the same time. The LBL approach tends to yield a higher standard deviation than the FSK approach, since similar random numbers may be inverted to very different emission wavenumbers, which results in quite different absorption during ray-tracing, while in the FSK method similar random numbers are inverted to similar g-values, resulting in similar absorption, due to the correlated-k assumption. However, such effects are hard to notice here since spectral uncertainty is only a minor contributor to the standard deviation. The same ray-tracing algorithm and finite-volume mesh used in the homogeneous problem were employed here and, thus, the computational times were the same.

While both LBL and FSK approaches yield comparable statistical errors, they are not equivalent in terms of accuracy. Since the LBL approach always uses exact local absorption coefficients in both emission and absorption calculations, the exact result can be achieved if a sufficient number of rays are traced. In contrast, the FSK approach uses approximated k-values based on the correlated-k assumption, which breaks down in this inhomogeneous problem, and results in significant errors compared to LBL results, as shown in Table 3. The FSK approach over-predicts total emission and averaged wall fluxes by around 10% in this problem.

To test the performance of PMC/LBL and PMC/FSK methods in more realistic scenarios, time-averaged cell-mean fields are obtained from the composition-PDF solution of a methane/air axisymmetric jet flame after statistical convergence has been achieved, and fed into the previous PMC solver. The flame is a scaled up Sandia Flame D [30] and has a central jet of methane and air mixed with a volume ratio of 1.3 at 293 K flowing into an open space at 24.8 m/s and the outer coflow of air is at 291 K and 0.45 m/s. Around the fuel jet an annular pilot flow of burnt gas enters at 1880 K and 5.7 m/s and the composition of the pilot gas is the equilibrium composition for burning of methane with an equivalence ratio of 0.77. The diameter of the fuel jet is $D = 14.4$ mm and the outer diameter of the pilot flow annulus is $2.62D$. The same computational domain and finite-volume mesh used in the homogeneous and the step-change problems are used again in the present problem. The P_1-approximation in conjunction with the FSK model was used to solve radiative transfer for the composition-PDF method [30]. Fig. 5 shows the time-averaged temperature and concentration fields. A one-step reaction mechanism is adopted in the PDF model and, as a result, the mole fraction ratio of products, water vapor and carbon dioxide, is constant everywhere and the uncorrelatedness of absorption coefficients is solely due to temperature variations. Again, the LBL and FSK approaches yield roughly the same statistical errors and 30,000 photon bundles per run are sufficient to resolve the spectral variation of radiative intensities, as shown in Table 4. Table 5 compares the LBL and FSK approaches in terms of total emission and boundary fluxes. FSK results are not exact again but errors are much smaller here than in the step-change case, which coincides with the observations of Zhang and Modest [23,24] as mentioned earlier.

It was also observed that the FSK approach is 3–4 times faster than the LBL approach, similar to the homogeneous case. However, the FSK approach requires additional time to prepare the random-number relations for all possible states after the reference state is determined. Since the

Table 3
Total emission and wall fluxes in the step-change problem; 50 × 2,000,000 rays and one wavenumber (or g) per ray

	Emission (W)	Averaged wall fluxes (W/cm^2)					
		$\bar{q}_1$	$\bar{q}_2$	$\bar{q}_3$	$\bar{q}_4$	$\bar{q}_5$	$\bar{q}_6$
LBL	54,747	0.646	0.790	0.790	0.646	0.946	0.946
FSK	62,075	0.714	0.875	0.875	0.714	1.04	1.04
Error (%)	13.4	10.5	10.8	10.8	10.5	9.94	9.94

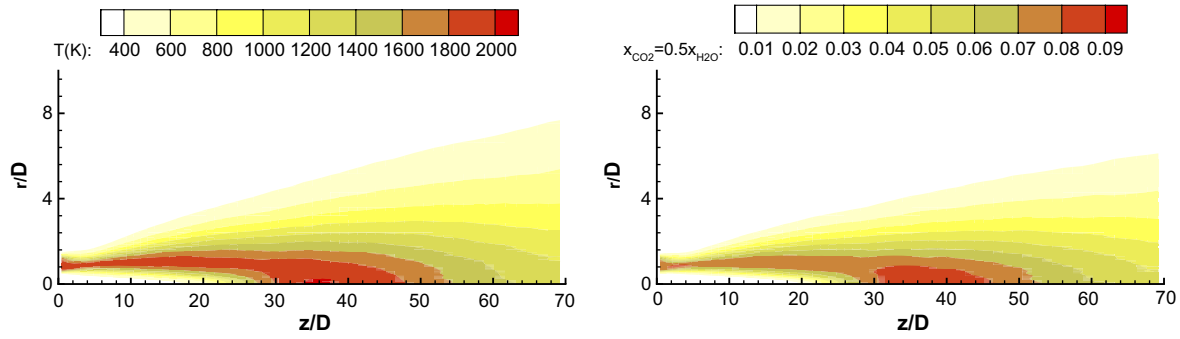

Fig. 5. Time-averaged cell-mean fields of temperature and concentrations.

Table 4
Relative standard deviations obtained in time-averaged cell-mean fields (50 runs)

N_{ray}	N_{wv}	Relative standard deviations (%)					
		σ_1	σ_2	σ_3	σ_4	σ_5	σ_6
(a) LBL approach							
30,000	1	1.59	1.18	1.09	0.97	2.08	1.42
	4	1.12	1.01	0.91	1.27	1.98	1.59
60,000	1	1.11	0.834	0.773	0.837	1.27	1.06
	4	1.02	0.659	0.650	1.04	1.69	1.07
120,000	1	0.691	0.532	0.450	0.557	1.02	0.73
(b) FSK approach							
30,000	1	1.34	1.04	1.17	1.06	1.96	1.66
	4	1.50	1.03	0.89	1.32	2.10	1.49
60,000	1	0.982	0.697	0.685	0.732	1.64	0.997
	4	1.01	0.765	0.654	0.941	1.62	0.950
120,000	1	0.621	0.530	0.457	0.586	1.14	0.785

typical computational times for assembling a full-spectrum k-distribution from the narrow-band k-distribution database is 0.1 s, for as few as 20 temperatures and 10 mole fractions for each of two species, setup time will require a minimum of 200 s.

Up to this point, PMC/LBL and PMC/FSK methods have been tested in continuum media using traditional ray-tracing methods. As mentioned earlier, media represented by discrete particle fields are also frequently encountered in combustion simulations using the PDF method. The PDF method was first developed by Pope [12] to treat chemical sources in turbulent reacting flows. Fluctuating scalars are treated as random variables and a differential equation predicting the probability-density-function for these scalars is generated. Because of its high dimensionality solutions to the PDF are found by a stochastic Monte Carlo approach, in which the fluid is modeled by a sufficiently large collection of fluid particles (point masses). Any turbulent quantity can then be evaluated exactly as long as it is a function of local scalars only (such as temperature and species concentrations). Wang and Modest [14] developed three absorption schemes, the Cone-PPM, Cone-SPM and Line-PPM schemes, by assigning a conical influence region to rays and/or a spherical influence region to particles, for ray-tracing in such media. All three absorption schemes are equivalent in terms of simulation accuracy. They also proposed an adaptive emission scheme to reduce statistical errors of PMC simulations, by splitting high particle energies and combining low particle energies to keep ray energies relatively constant [15]. The present PMC/LBL and PMC/FSK methods have also been incorporated into the above absorption and emission schemes to deal with media represented by particle fields. In the present paper the Cone-PPM scheme is adopted for sample calculations and the recommended value of a 1° ray opening angle is used.

A snapshot of a particle field containing roughly 80,000 stochastic particles is extracted from the particle Monte Carlo solution of the composition-PDF simulation of the scaled Sandia D flame [30], which was already used in the previous example. The turbulence scale in a turbulent jet flame depends on the properties of the fuel jet and the Reynolds number based on the fuel jet is essential in characterizing turbulent flows. In the present flame the Reynolds number is 22,400. The scale of the radiation field is generally characterized by the optical thickness, which is calculated based on the Planck-mean absorption coefficient of the combustion products and the flame length. The optical thickness of the present flame is 0.474. Fig. 6 shows the cell-mean values of temperature and CO_2 mole fraction. Again, because of the one-step reaction mechanism used in the

Table 5
Total emission and boundary fluxes in time-averaged cell-mean fields; 50 × 2,000,000 rays and one wavenumber (or g) per ray

	Emission (W)	Averaged wall fluxes (W/cm^2)					
		$\bar{q}_1$	$\bar{q}_2$	$\bar{q}_3$	$\bar{q}_4$	$\bar{q}_5$	$\bar{q}_6$
LBL	3513	0.0580	0.104	0.116	0.0775	0.0646	0.0753
FSK	3589	0.0582	0.105	0.117	0.0771	0.0641	0.0733
Error (%)	2.16	0.34	0.96	0.86	−0.52	−0.77	−2.66

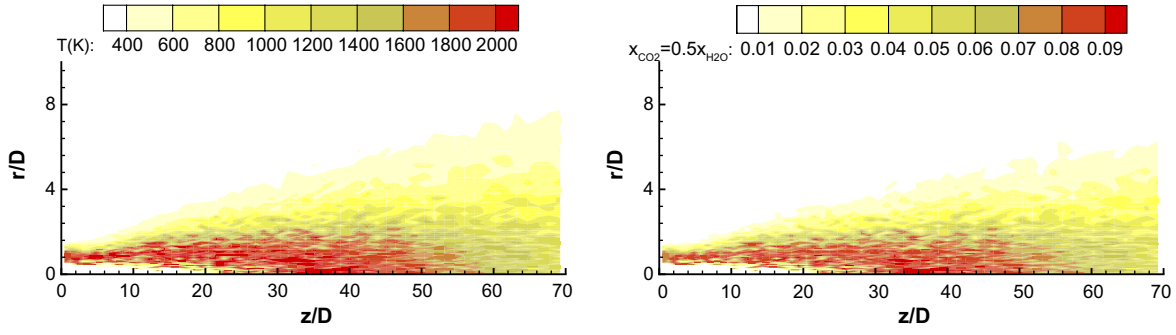

Fig. 6. Cell-mean contours of temperature and concentrations calculated from a snapshot of particle fields.

simulation, the ratio of mole fractions of CO_2 and H_2O is constant everywhere. The roughness of cell-mean fields implies large local gradients of temperature and mole fractions. Fig. 6 is only a single snapshot of cell-mean values, which fluctuate with time indicating a turbulent medium. By time-averaging over all snapshots, the time-averaged cell-mean fields can be obtained as given in Fig. 5. Interactions between turbulence and radiation tend to enhance the heat loss. Effects of turbulence–radiation interactions (TRI) may be investigated with such "frozen" particle field. In treatments of TRI using deterministic methods, only the coupling between radiative emission and local fluctuating absorption coefficients, "emission TRI", can be considered, and the coupling between incoming radiative intensities and local absorption coefficients, "absorption TRI", is ignored by applying the so-called optically-thin-fluctuation assumption (OTFA) [31]. However, in joint-PDF methods, the instantaneous scalar fields are known and represented by particle fields evolving with time, and the TRI can be fully calculated if a photon Monte Carlo simulation is used to determine radiation. If properties of the individual stochastic particle (temperature and absorption coefficient) are employed in both emission and absorption calculations, both emission TRI and absorption TRI are taken into account, labeled here "full-TRI." If properties of the individual stochastic particle are used in emission calculations, but cell-mean values are used in absorption calculations, then only the emission TRI is taken into account (equivalent to the OTFA assumption), called here "partial-TRI." If cell-mean values are used in both emission and absorption calculations, turbulence–radiation interactions are neglected entirely.

Relative standard deviations of boundary fluxes and the averaged CPU time are compared in Table 6 for the LBL and FSK approaches using various amounts of rays per run and wavenumbers per ray. It is observed that 30,000 rays per run are sufficient to resolve the spectral uncertainty and the spacial uncertainty dominates the statistical error once again for both LBL and FSK approaches in this turbulent particle field. However, if the cell-based heat source terms are desired, as required in the energy equation in combustion modeling, a much higher number of rays will be needed to achieve the same level of statistical error in terms of heat source, considering that the scale of finite-volume cells is generally much smaller than that of the six surfaces under investigation here. Unlike previous cases, the difference in CPU-time efficiency between the LBL and FSK approaches is not substantial, because the ray–particle interaction is the most time-intensive part in the Monte Carlo simulations in particle fields, making the difference between spectral models less prominent. Table 7 shows that the FSK approach over-estimates the total emission from the particle field by about 2% and under-estimates the total heat loss by 6% due to the inaccuracy of the correlated-k assumption, which leads to an over-estimation of absorption (emission minus heat loss) by around 16%. The gray analysis, on the other hand, in which local Planck-mean absorption coefficients are used in both emission and absorption calculations, over-estimates the total heat loss by over 50%.

Effects of turbulence–radiation interactions were also investigated for the above particle field. Table 8 lists the total emission and total heat loss for the three different TRI treatments. The PMC/LBL method was employed in all cases. It is observed that total emission is under-estimated by 14% if TRI is neglected, showing that emission TRI must be taken into account in the present turbulent jet flame. However, there is only a negligible difference

Table 7
Total emission and heat loss from particle field for different spectral models (in W; 50 × 200,000 rays)

	Emission	Heat loss	
		Mean	Error (%)
LBL	4920	3029	–
FSK	5034	2847	−6.0
Gray	4920	4589	51.5

Table 6
Relative standard deviations of wall fluxes and averaged CPU time per simulation; 50 runs; particle field

N_{ray}	N_{wv}	Relative standard deviations (%)						t_{cpu} (s)
		σ_1	σ_2	σ_3	σ_4	σ_5	σ_6	
(a) LBL approach								
30,000	1	1.56	1.09	0.923	1.25	2.28	1.61	13.4
	4	1.22	1.20	0.979	1.20	2.29	1.62	19.2
60,000	1	1.11	0.826	0.796	0.918	1.69	1.31	27.7
	4	1.11	0.871	0.757	0.782	1.37	0.870	36.6
120,000	1	0.776	0.627	0.558	0.635	1.16	0.993	48.3
(b) FSK approach								
30,000	1	1.84	1.44	1.13	1.40	2.30	1.97	10.7
	4	1.97	1.24	1.09	1.56	2.38	2.65	13.6
60,000	1	1.28	0.720	0.743	0.987	1.96	1.52	21.0
	4	1.17	0.987	0.806	1.06	1.95	1.31	26.0
120,000	1	0.751	0.652	0.577	0.678	1.23	1.06	42.9

Table 8
Total emission and heat loss from particle field for different TRI treatments(in W; 50 × 200,000 rays)

	Emission	Heat loss	
		Mean	Error (%)
Full-TRI	4920	3029	–
Partial-TRI	4920	3019	−0.33
No-TRI	4270	2471	−18.4

between the full-TRI and the partial-TRI treatments in the heat loss estimation, which implies that absorption TRI is negligible and the OTFA assumption is valid in the present flame model. This was to be expected since, though absorption TRI may be appreciable in some small parts of the spectrum where absorption coefficients are large, the overall effect is still expected to be minimal after integration over the entire spectrum, as pointed out by Hartick [32].

From the above sample calculations one observes that both PMC/LBL and PMC/FSK approaches result in roughly the same level of statistical errors in both homogeneous and inhomogeneous media for the same number of rays. By using the random-number–wavenumber relation, the LBL method does its own spectral reordering, in effect similar to the FSK reordering. The spectral behavior can be resolved with a limited number of rays while spacial uncertainty is the major contributor to statistical errors. The FSK approach is superior in CPU-time efficiency over the LBL approach, but this advantage is diminished in media represented by particle fields due to the time-intensive ray-tracing process. Because of the time-consuming database preparation the FSK approach also becomes less CPU efficient in quickly-evolving media.

5. Summary

Spectral LBL and FSK approaches have been incorporated into PMC models to calculate radiative heat transfer in nongray combustion gases. Random-number relations are formulated for gaseous mixtures, which can be calculated efficiently based on individual species random-number relations, and such databases were constructed for water vapor and carbon dioxide, the two most important combustion gases, using pressure-based absorption coefficients. While much more memory efficient than the LBL approach, the FSK method is not promising in terms of CPU-time efficiency, since the calculational effort of the FSK algorithm increases exponentially with the number of species, while that of the LBL algorithm increases only linearly. Considering the time-consuming database preparation process, the FSK method is not suitable for quickly-evolving media. In contrast, the LBL method does not require such a preparation process since the LBL database can be constructed once and for all.

By using random-number relations, the wavenumbers contributing the most to radiation have higher probabilities to be chosen during PMC simulations, which is equivalent to spectral reordering in the FSK method. Thus, it was observed that both the LBL and FSK approaches produce the same level of statistical errors for a given number of photon bundles in various sample cases, including both a homogeneous problem and inhomogeneous problems, and both continuum media and a medium represented by discrete particle fields. A relatively small number of rays can resolve the spectral uncertainty in PMC simulations for both LBL and FSK methods. However, the FSK method has inherent inaccuracy in inhomogeneous media since absorption coefficients are not truly correlated. Turbulence–radiation interactions in a methane/air jet flame were also investigated using the proposed PMC/LBL method. It is noted that the PMC method for stochastic media is the only method that allows the full evaluation of TRI, including the so-called absorption TRI.

Acknowledgment

This research has been sponsored by National Science Foundation under Grant Number CTS-0121573.

References

[1] J.R. Howell, M. Perlmutter, Monte Carlo solution of thermal transfer through radiant media between gray walls, J. Heat Transfer 86 (1) (1964) 116–122.
[2] M.F. Modest, The Monte Carlo method applied to gases with spectral line structure, Numer. Heat Transfer B 22 (3) (1992) 273–284.
[3] J. Liu, S.N. Tiwari, Investigation of radiative transfer in nongray gases using a narrow band model and Monte Carlo simulation, J. Heat Transfer 116 (1) (1994) 160–166.
[4] M. Cherkaoui, J.-L. Dufresne, R. Fournier, J.-Y. Grandpeix, A. Lahellec, Monte Carlo simulation of radiation in gases with a narrow-band model and a net-exchange formulation, J. Heat Transfer 118 (2) (1996) 401–407.
[5] J.T. Farmer, J.R. Howell, Monte Carlo prediction of radiative heat transfer in inhomogeneous, anisotropic, nongray media, J. Thermophys. Heat Transfer 8 (1) (1994) 133–139.
[6] J.T. Farmer, J.R. Howell, Comparison of Monte Carlo strategies for radiative transfer in participating media, in: J.P. Hartnett, T.F. Irvine (Eds.), Advances in Heat Transfer, vol. 31, Academic Press, New York, 1998.
[7] L. Wang, J. Yang, M.F. Modest, D.C. Haworth, Application of the full-spectrum *k*-distribution method to photon Monte Carlo solvers, J. Quant. Spectrosc. Radiat. Transfer 104 (2) (2006) 297–304.
[8] K.C. Tang, M.Q. Brewster, Analysis of molecular gas radiation: real gas property effects, J. Thermophys. Heat Transfer 13 (4) (1999) 460–466.
[9] A.Y. Snegirev, Statistical modeling of thermal radiation transfer in buoyant turbulent diffusion flames, Combust. Flame 136 (2004) 51–71.
[10] L. Tessé, F. Dupoirieux, B. Zamuner, J. Taine, Radiative transfer in real gases using reciprocal and forward Monte Carlo methods and a correlated-*k* approach, Int. J. Heat Mass Transfer 45 (2002) 2797–2814.
[11] Lionel Tessé, Francis Dupoirieux, Jean Taine, Monte Carlo modeling of radiative transfer in a turbulent sooty flame, Int. J. Heat Mass Transfer 47 (2004) 555–572.
[12] S.B. Pope, PDF methods for turbulent reactive flows, Prog. Energy Combust. Sci. 11 (1985) 119–192.

[13] S. Subramaniam, D.C. Haworth, A PDF method for turbulent mixing and combustion on three-dimensional unstructured deforming meshes, J. Engine Res. 1 (2000) 171–190.
[14] A. Wang, M.F. Modest, Photon Monte Carlo simulation for radiative transfer in gaseous media represented by discrete particle fields, J. Heat Transfer 128 (10) (2006) 1041–1049.
[15] A. Wang, M.F. Modest, An adaptive emission model for Monte Carlo ray-tracing in participating media represented by statistical particle fields, J. Quant. Spectrosc. Radiat. Transfer 104 (2) (2007) 288–296.
[16] X.L. Xia, D.P. Ren, H.P. Tan, A curve Monte Carlo method for radiative heat transfer in absorbing and scattering gradient-index medium, Numer. Heat Transfer, Part B: Fundam. 50 (2) (2006) 181–192.
[17] L.M. Ruan, H.P. Tan, Y.Y. Yan, A Monte Carlo (MC) method applied to the medium with nongray absorbing–emitting-anisotropic scattering particles and gray approximation, Numer. Heat Transfer, Part A: Appl. 42 (3) (2002) 253–268.
[18] S. Mazumdar, A. Kersch, A fast Monte Carlo scheme for thermal radiation in semiconductor processing applications, Numer. Heat Transfer, Part B: Fundam. 37 (2) (2000) 185–199.
[19] M.F. Modest, S.C. Poon, Determination of three-dimensional radiative exchange factors for the space shuttle by Monte Carlo, ASME Paper No. 77-HT-49, 1977.
[20] M.F. Modest, Determination of radiative exchange factors for three dimensional geometries with nonideal surface properties, Numer. Heat Transfer 1 (1978) 403–416.
[21] M.F. Modest, Radiative Heat Transfer, second ed., Academic Press, New York, 2003.
[22] M.F. Modest, Narrow-band and full-spectrum *k*-distributions for radiative heat transfer—correlated-*k* vs. scaling approximation, J. Quant. Spectrosc. Radiat. Transfer 76 (1) (2003) 69–83.
[23] M.F. Modest, H. Zhang, The full-spectrum correlated-*k* distribution for thermal radiation from molecular gas–particulate mixtures, J. Heat Transfer 124 (1) (2002) 30–38.
[24] H. Zhang, M.F. Modest, A multi-scale full-spectrum correlated-*k* distribution for radiative heat transfer in inhomogeneous gas mixtures, J. Quant. Spectrosc. Radiat. Transfer 73 (2–5) (2002) 349–360.
[25] S.A. Tashkun, V.I. Perevalov, J.-L. Teffo, A.D. Bykov, N.N. Lavrentieva, CDSD-1000, the high-temperature carbon dioxide spectroscopic databank, J. Quant. Spectrosc. Radiat. Transfer 82 (1–4) (2003) 165–196. <ftp://ftp.iao.ru/pub/CDSD-1000>.
[26] M.F. Modest, S.P. Bharadwaj, High-resolution, high-temperature transmissivity measurements and correlations for carbon dioxide–nitrogen mixtures, J. Quant. Spectrosc. Radiat. Transfer 73 (2–5) (2002) 329–338.
[27] A. Wang, M.F. Modest, Importance of combined Lorentz–Doppler broadening in high-temperature radiative heat transfer applications, J. Heat Transfer 126 (5) (2004) 858–861.
[28] A. Wang, M.F. Modest, High-accuracy, compact database of narrow-band *k*-distributions for water vapor and carbon dioxide, J. Quant. Spectrosc. Radiat. Transfer 93 (2005) 245–261.
[29] M.F. Modest, Computer Codes for Radiative Heat Transfer, second ed., Academic Press, New York, 2003. <http://www.bh.com/companions/0125031637>.
[30] G. Li, M.F. Modest, Importance of turbulence–radiation interactions in turbulent diffusion jet flames, J. Heat Transfer 125 (2003) 831–838.
[31] V.P. Kabashnikov, G.I. Myasnikova, Thermal radiation in turbulent flows—temperature and concentration fluctuations, Heat Transfer—Sov. Res. 17 (6) (1985) 116–125.
[32] J.W. Hartick, M. Tacke, G. Fruchtel, E.P. Hassel, J. Janicka, Interaction of turbulence and radiation in confined diffusion flames, in: Twenty-Sixth Symposium (International) on Combustion, The Combustion Institute, 1996, pp. 75–82.